Dysregulation of autoreactive B cell responses in autoimmune diseases: from initial triggering to persistent activation

Neppelenbroek, S.


4

CHAPTER 4

Enhanced recognition of topoisomerase 1 upon DNA binding by a subset of anti-topoisomerase 1 autoantibodies in systemic sclerosis

Sam Neppelenbroek[1], Corrie M. Wortel[1], Danique M.H. van Rijswijck[2], Marjolein J.A.L. Wetzels[1], Robbert Q. Kim[3], E.W. Nivine Levarht[1], Albert J.R. Heck[2], Jeska K. de Vries-Bouwstra[1], Cynthia M. Fehres[1], René E.M. Toes[1], Hans U. Scherer[1]

[1] Department of Rheumatology, Leiden University Medical Center, Leiden, The Netherlands
[2] Biomolecular Mass Spectrometry and Proteomics, Bijvoet Center for Biomolecular Research and Utrecht Institute for Pharmaceutical Sciences, Utrecht University, Utrecht, The Netherlands.
[3] Protein Facility, Department of Cell and Chemical Biology, Leiden University Medical Center, Leiden, The Netherlands

Key messages:

What is already known on this topic:

- Autoantibodies targeting topoisomerase 1 (TOP1) associate with disease phenotype and severity of organ complications in systemic sclerosis.
- Activated, TOP1-reactive memory B cells and TOP1-secreting plasma cells are found in the circulation of patients with progressive disease and those with pulmonary fibrosis.

What this study adds:

- Novel evidence describing anti-TOP1 monoclonal autoantibodies (ATA) derived from SSc patients which are heterogeneous and differentially recognize TOP1 and TOP1 in complex with DNA.
- TOP1-DNA complexes enhance the recognition by some but not all anti-TOP1 autoantibodies, a phenomenon observed in most patients.
- The differential recognition of TOP1 and TOP1-DNA complexes affects the immunostimulatory properties of ATA.

How this study might affect research, practice or policy:

- Differential recognition patterns of ATA indicate functional heterogeneity in the B cell response targeting TOP1, which may help to further dissect and understand patient and disease heterogeneity.
- DNA binding by TOP1 could be an important determinant in the activation of the ATA B cell response and thereby offers new insights in potential drivers of disease-relevant immunological processes.

Keywords: Systemic sclerosis, anti-topoisomerase 1 autoantibodies, topoisomerase 1, topoisomerase 1-DNA cleavage complexes.

Abstract:

Objectives

Systemic sclerosis (SSc) is a deleterious disease. Its clinical management is complicated by strong interpatient heterogeneity. Progressive organ fibrosis is linked to autoantibodies against topoisomerase 1 (TOP1). Here, we hypothesized that the molecular interaction between anti-TOP1 autoantibodies (ATAs) and TOP1 could be a relevant determinant of SSc pathogenesis. DNA binding by TOP1 might affect its interaction with ATAs. Therefore, we studied the effect of DNA binding by TOP1 on ATA recognition.

Methods

ATA monoclonal antibodies (ATA mAbs) were generated from patient-derived TOP1-reactive B cells. Reactivity of ATA mAbs and antibodies in patient plasma towards TOP1 and TOP1-DNA cleavage complexes (TOP1cc) was determined by ELISA and mass photometry. Immunostimulatory properties of ATA mAbs in complex with TOP1/TOP1cc were assessed by stimulation of monocytic THP-1 cells.

Results

DNA binding by TOP1 differentially affected the recognition of TOP1 by ATA mAbs. A subset of mAbs showed enhanced binding to TOP1cc, whereas others recognized TOP1 and TOP1cc to a similar extent. ATAs with enhanced TOP1cc recognition were observed in plasma of ATA^+ SSc patients and correlated with ATA levels and interstitial lung disease. These 'TOP1cc-enhanced ATAs' variably affected the enzymatic function of TOP1 and circulated predominantly as IgG1 and IgM. The interaction of 'TOP1cc-enhanced ATA mAbs' with TOP1cc strongly increased IL-8 production by THP-1 cells.

Conclusions

The differential recognition of TOP1 upon DNA binding by ATAs demonstrates heterogeneity in the ATA B cell response, possibly impacting on disease-relevant processes in severe SSc.

Available as preprint on *BioRxiv, 2025.05.26.656088*

Introduction

Systemic sclerosis (SSc) is a heterogeneous disease characterized by fibrosis of internal organs and the skin, vasculopathy and autoimmunity. The disease displays remarkable clinical heterogeneity ranging from indolent to rapidly progressive disease with irreversible organ damage and subsequent mortality. Clinical management of SSc is complicated by the lack of effective treatments and variation in disease progression, which is difficult to predict[1]. Therefore, identification of pathogenic mechanisms driving disease may improve patient stratification and enable the development of targeted treatment strategies.

Like many other autoimmune diseases, SSc is hallmarked by a break in B cell tolerance towards nuclear proteins[2,3]. Autoantibodies targeting the nuclear enzyme topoisomerase 1 (TOP1) are observed in a subset of SSc patients and associate with diffuse cutaneous SSc, a distinct clinical phenotype with the highest mortality among the rheumatic diseases[4,5]. Specifically, anti-topoisomerase 1 autoantibodies (ATAs) associate with progressive lung and skin fibrosis and early death, although not all ATA-positive patients show this progressive course of disease[6]. Recently, we could associate measures reflective of an active ATA B cell response to disease progression in ATA$^+$ SSc patients[7,8]. Specifically, ATA-secreting B cells were found in the circulation of SSc patients and their presence associated with the presence and severity of pulmonary fibrosis[7]. Also, the presence of ATA-IgM was predictive of disease progression in the early stages of disease[8]. These findings suggest that activated, autoreactive ATA B cells might contribute directly to processes driving fibrosis. This notion is further supported by the beneficial effects of B cell-targeting therapies in SSc[9,10]. Nevertheless, the mechanisms by which ATA B cells could contribute to disease remain unclear[3]. ATA pathogenicity has been debated, with the hypothesis that ATAs directly activate fibroblasts[11–13]. However, whether this affects disease *in vivo* is unclear, primarily because ATA can also be present in indolent disease. ATA B cells, on the other hand, might contribute to disease by the production of cytokines and stimulation of T cells through antigen presentation and co-stimulation[14].

A crucial prerequisite for B cell activation is the recognition of antigen by B cell receptors (BCR)[15,16]. The same holds for antibody-mediated effector functions which require antibody-binding to cognate antigens. Epitope structure and conformation can determine and modulate these interactions[17]. TOP1 is a DNA-binding nuclear protein which unwinds negatively supercoiled DNA[18]. During its enzymatic cycle, TOP1 covalently binds DNA to form a TOP1-DNA cleavage complex (TOP1cc) which allows the passing of the other DNA strand through the single-stranded break[18]. TOP1cc is a transient complex under physiological conditions, but stable TOP1cc can be formed if DNA contains lesions, which can occur during cell death induced under inflammatory conditions[19]. Binding of antigen to nucleic acids, a common property among many nuclear antigens targeted in autoimmune diseases, can potentiate antibody effector functions and B cell activation through co-engagement of innate Toll-like receptors with Fc receptors or the BCR[2,16]. Whether TOP1 as SSc autoantigen binds DNA, and how TOP1 and TOP1cc are recognized by human ATAs, warrants detailed analyses to better understand the antigenicity of TOP1 in SSc pathogenesis.

To this end, we set out to determine the molecular and functional characteristics of the

interaction between ATAs and TOP1. We generated patient-derived monoclonal ATAs (ATA mAbs) enabling us to study the effect of DNA binding by TOP1 on the interaction with ATAs. We found remarkable heterogeneity in the recognition of TOP1 and TOP1cc among ATA mAbs and ATA in plasma. This heterogeneity affected antibody functionality and likely impacts on disease-relevant processes in progressive SSc. Together, these findings contribute to our understanding of disease variability in ATA$^+$ SSc.

Methods

The experimental procedures for the recombinant production and purification of human TOP1, the generation of patient-derived ATA mAbs, gel electrophoresis, western blotting, cross-inhibition ELISA with ATA mAbs, mass photometry and TOP1-mediated DNA relaxation assay are provided in detail in the supplementary methods section.

Patients and healthy individuals

Peripheral blood was obtained from ATA$^+$ and anti-centromere protein B autoantibody (ACA)$^+$ SSc patients visiting the outpatient clinic of the Department of Rheumatology at Leiden University Medical Center. These SSc patients were included in the Leiden Combined Care in Systemic Sclerosis (CCISS) cohort[20], fulfilled the ACR/EULAR 2013 classification criteria for SSc and were either ATA-IgG$^+$ or ACA-IgG$^+$ as measured by routine clinical diagnostic tests. Patients on B-cell depleting therapies or patients with a history of hematopoietic stem cell transplantation were excluded. Plasma samples of a cross-sectional cohort of ATA-IgG$^+$ SSc patients (n=21) collected in a previous study were used (Table 1)[7]. In addition, serum samples of ATA-IgG$^+$ SSc patients containing high levels of ATA-IgM (n=9) were selected from another previously reported study (Table 1)[8]. Plasma samples from ACA$^+$ SSc patients (n=9) and healthy donors (n=6) were used as controls (Table 1).

Table 1. Characteristics of ATA$^+$ and ACA$^+$ SSC patients and healthy donors

	ATA-IgG$^+$ SSC patients (n=21)	ATA-IgM^{high} SSC patients (n=9)	ACA-IgG$^+$ SSC patients (n=9)	Healthy donors (n=6)
Age years, median (IQR)	55 (39-65)	53 (36-67)	55 (46-68)	29 (26-36)
Sex female, n (%)	11 (52%)	8 (89%)	9 (100%)	5 (83%)
Duration since first NRP symptom, months, median (IQR)	56 (31-92.8)	48 (14.5-119)	117 (57-359)	
Diffuse cutaneous SSc n (%)	7 (33%)	3 (33%)	0 (0%)	
mRSS median (IQR)	5 (2-7.5)	6 (4-16)	5 (0-9)	
ILD on HRCT n (%)	14 (66.7%)	8 (89%)	0 (0%)	
Current use of Immunosuppressive drugs n (%)	12 (57%)	1 (11%)	3 (33%)	

IQR = interquartile range, NRP = non-Raynaud's phenomenon, mRSS = modified Rodnan skin score, ILD = interstitial lung disease, HRCT = high-resolution computer tomography scan.

Generation of TOP1cc using suicide substrate

To obtain stable TOP1-DNA cleavage complexes (TOP1cc), TOP1 was incubated with a suicide substrate (ScS) which is covalently bound by TOP1. Suicide substrate was generated as described previously by Kristoffersen *et al*[21]. Three oligonucleotides (26DL: '5-pAGA AAA ATT TTT CCG AGT GCG AAG-3' (p = phosphorylated 5'), 38SC: 5'-CTA GAG GAT CTA AAA GAC TTA GA-3', 61NCL: 5'-CTT CGC ACT CGG AAA AAT TTT TCT AAG TCT TTT AGA TCC TCT AG-3') were mixed to obtain a 66.67µM concentration of ScS. The suspension was heated to 80°C for 5 minutes and cooled to room temperature in 3 hours. TOP1cc was formed by incubation of 0.1mg/ml of TOP1 with 5µM of ScS for 30 minutes at 37°C.

Anti-TOP1/TOP1cc-antibody ELISAs

To measure the reactivity of ATA mAbs and antibodies in plasma towards TOP1 and TOP1cc, high binding 384-well microplates (Corning) were coated with 2.5µg/ml TOP1 or TOP1cc in PBS (pH=8). Plates were blocked using 1% BSA in PBS (Ig, IgG, IgG subclasses and IgA) or 1% skim milk in PBS (IgM). Plasma, ATA mAbs and culture supernatants of single cell cultured B cells were applied in single or serial dilutions (as indicated in the respective figures) in 1% BSA in PBS with 0.05% Tween (Ig, IgG, IgG subclasses and IgA) or in 1% skim milk in PBS with 0.05% Tween (IgM). Subsequently, secondary antibodies were added: rabbit anti-human IgG-HRP (1:5000, P0214, DAKO), mouse anti-human IgG1 (1:5000, HP6186, Nordic-MUbio), mouse anti-human IgG2 (1:250, HP6014, Nordic-MUbio), mouse anti-human IgG3 (HP6080, 1:2500, Nordic-MUbio), mouse anti-human IgG4 (1:500, MH164-1, Sanquin), goat anti-human IgA-HRP (1:1000, A18781, Novex), goat anti-human-IgM-HRP (1:5000, AP114P, Millipore), and goat anti-human Ig-HRP (1:10000, A80-152P, Bethyl Laboratories). Goat anti-mouse Ig-HRP (1:5000 for IgG1/2, 1:2500 for IgG3/4, P0447, DAKO) was used to detect the IgG subclass-specific, secondary antibodies. Pooled plasma samples were used as reference standards. ATA mAbs were used in all plasma ELISAs to control for comparable coating of TOP1 and TOP1cc (ATA mAb 2F8) and as positive controls for the differential recognition of TOP1cc compared to TOP1 (ATA mAbs 7G6 and 9D11). ELISAs were developed using ABTS supplemented with H_2O_2. Optical density was measured at 415 nanometers with a Spectramax I3x Multi-Mode Microplate Reader (Molecular Devices) using SoftMax® Pro 7 (version 7.0.2, Molecular Devices).

Stimulation of THP-1 cells

To assess the immunostimulatory properties of ATA mAbs, monocytic THP-1 cells were stimulated with ATA mAbs in complex with plate-bound TOP1 or TOP1cc. NUNC Maxisorp 96-well plates (ThermoFisher Scientific) were coated with 5µg/ml TOP1 and TOP1cc. Plates were blocked with PBS 1% BSA and 2.5µg/ml of LPS-depleted (Pierce™ High Capacity Endotoxin Removal Spin Columns, ThermoFisher Scientific), sterile-filtered ATA mAbs were subsequently added to the plates. The anti-citrullinated protein mAb 1F2 was used as negative control[22]. Upon the formation of plate-bound immune complexes, $1x10^5$ THP1 cells were added to the plates and stimulated for 24 hours at 37°C, 5% CO_2. Stimulation with 1µg/ml lipopolysaccharide (LPS, Sigma) served as positive control. Upon stimulation, culture supernatants were collected to determine the secretion of IL-8 by the THP-1 cells.

IL-8 ELISA

Human IL-8 was measured using a commercial ELISA on culture supernatants of THP-1 cells

in accordance with the manufacturer's instructions (DY208-05, R&D Systems). Volumes of the ELISA were adapted for the use of high binding 384-well Microplates (Corning): 15µl for coating, sample, and BD OptEIATM TMB substrate solution (555214, BD Biosciences), 75µl for blocking (1% BSA in PBS), and 7.5µl for stop solution (1M H_2SO_4). Reactions were developed for 50 minutes and absorbance was measured with a Spectramax I3x Multi-Mode Microplate Reader (Molecular Devices) at 450 nanometers with correction of the absorbance at 570nm.

Statistical analysis

Data were analyzed using Graphpad Prism (version 10.2.3). As indicated in the figure legends, Mann-Whitney U test, Wilcoxon matched-pairs signed rank test, and Kruskal-Wallis test combined with Dunn's multiple comparison were used where appropriate to determine the statistical significance of the data. Correlations were described using Spearman's rank correlation coefficient (r_s).

Study approval

This study was approved by the ethical review board of the Leiden University Medical Center (protocol number P17.151) and the Leiden University Biobank Toetsing Commissie (REU/036/SH/sh). Included patients gave written informed consent to participate in the study.

Results

Generation and characterization of patient-derived anti-topoisomerase 1 monoclonal antibodies

We first generated ATA mAbs based on BCR sequences of TOP1-reactive B cells obtained from an ATA$^+$ SSc patient. B cells from peripheral blood of the patient were single cell sorted based on their reactivity towards TOP1 conjugated to Alexa Fluor™ 647 and phycoerythrin (Fig. 1A). These sorted cells were subsequently differentiated towards antibody-secreting cells in culture. Secreted antibodies could be detected in a fraction of the culture supernatants (Suppl. Fig. S1A-C). By analyzing the reactivity of the secreted antibodies towards human TOP1, we identified several TOP1-reactive clones (Fig. 1B-D).

Table 2. B cell receptor sequence details of patient-derived ATA mAbs

Clone	HC	IGHV	IGHV mutations (#)	IGHV identity (%)	IGHD	IGHJ	IGH-CDR3	LC	IGK/LV	IGK/LV mutations (#)	IGK/LV identity (%)	IGK/L-CDR3
2F8	IGHA1	V1-18	14	95.14	D6-6	J4	CARGRDFSSSPYDYW	λ	V3-21	7	J2/J3	CQVWDRSSDDVIF
7G6	IGHG1	V3-48	26	90.97	D6-6	J5	CATTPRTGRPW	κ	V4-1	12	J4	CQQYLTPLQIF
9D11	IGHG3	V1-3	28	93.75	D2-15	J4	CARDGGSSVAVISATLDSW	λ	V2-23	8	J2/J3	CCSYAGSRGVVF

HC = heavy chain, IGHV = heavy chain V gene, IGHV mutations (#) = amount of nucleotide mutations in IGHV compared to closest germline IGHV, IGHV identity (%) = similarity of IGHV compared to closest germline IGHV expressed in a percentage, IGHD = heavy chain D gene, IGHJ = heavy chain J gene, IGH-CDR3 = amino acid sequence of heavy chain complementarity-determining region 3, LC = light chain, κ = kappa, λ = lambda, IGK/LV = light chain V gene, IGK/LV mutations (#) = amount of nucleotide mutations in IGK/LV compared to germline IGK/LV, IGK/LV identity (%) = similarity of IGK/LV compared to germline IGK/LV expressed in a percentage, IGK/LJ = light chain J gene, IGK/L-CDR3 = amino acid sequence of light chain complementarity-determining region 3.

BCR sequences were determined from three of these clones (termed 2F8, 7G6 and 9D11; Table 2) and expressed recombinantly as IgG1 mAbs (Suppl. Fig. S1D). Reactivity of the

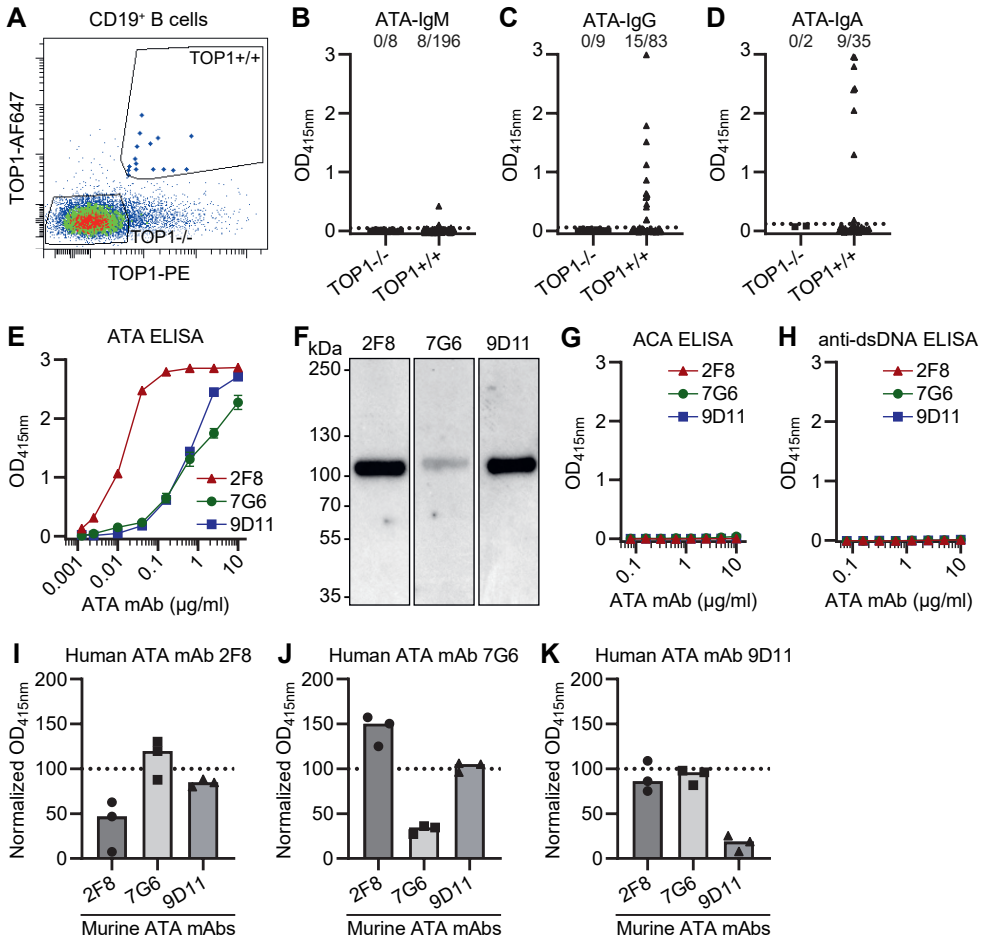

Figure 1. Generation and characterization of patient-derived ATA mAbs. (A) Gating strategy used to single-cell sort CD19^{+} TOP1$^{+/+}$ B cells binding to TOP1-Alexa Fluor™ 647 (AF647) and TOP1-phycoerythrin (PE). **(B-D)** Reactivity of IgM **(B)**, IgG **(C)** and IgA **(D)** secreted by single-cell-sorted TOP1$^{+/+}$ B cells towards TOP1 as assessed by an anti-TOP1-Ig (ATA-IgM), anti-TOP1-IgG and anti-TOP1-IgA ELISA, respectively. Cut-off (mean TOP1$^{-/-}$ B cells + 4x standard deviation) is represented by dotted line. Only culture supernatants in which IgM, IgG or IgA could be detected (Suppl. Fig. 1A-C) are depicted. **(E)** Reactivity of patient-derived ATA mAbs towards TOP1 in an ATA-IgG ELISA. **(F)** Binding of TOP1 by ATA mAbs on western blot. Molecular weight in kilodaltons (kDa) was estimated using a protein ladder. **(G-H)** Reactivity of ATA mAbs towards centromere protein B in an anti-centromere protein B antibody-IgG (ACA-IgG) ELISA **(G)** and towards double-stranded DNA in an anti-double-stranded DNA-IgG (anti-dsDNA-IgG) ELISA **(H)**. **(I-K)** Binding of ATA mAbs 2F8 **(I)**, 7G6 **(J)** and 9D11 **(K)** with a human constant domain (human ATA mAbs) to a TOP1-coated ELISA plate pre-incubated with 5µg/ml of the indicated ATA mAbs with a murine constant domain (murine ATA mAbs). Binding was normalized to condition in which no murine mAb was added. Concentrations of human mAbs were in the linear range of the ATA-IgG ELISA; 2F8 - 0.04µg/ml, 7G6 & 9D11 - 1µg/ml. Data is derived from three independent experiments. **(B-E, G-K)** Optical density was measured at 415 nanometers (OD_{415nm}). **(E, G-H)** Error bars represent standard deviation of technical duplicates. **(E-H)** Data are representative of at least two independent experiments.

generated ATA mAbs towards TOP1 was verified by ELISA in a concentration-dependent manner (Fig. 1E). TOP1 binding by ATA-IgG 2F8 was stronger compared to ATA-IgGs 7G6 and 9D11. Specificity of ATA mAbs was further confirmed by western blotting, with all ATA mAbs recognizing one band at the expected height of TOP1 (Fig. 1F, Suppl. Fig. S1E). No binding was observed to centromeric protein B (CENP-B) and double-stranded DNA (Fig. 1G-H).

We also performed cross-inhibition assays to determine whether the recombinantly produced ATA mAbs would bind unique or overlapping TOP1 epitopes. The three ATA mAbs were generated with murine constant domains to test their capacity to inhibit TOP1 binding by ATA mAbs with a human constant domain. Binding of human ATA mAbs to TOP1 could be blocked by their direct murine counterparts, but not by the respective other mAbs (Fig. 1I-K, Suppl. Fig. S1F). Together, these data show that we generated three ATA mAbs binding unique epitopes of human TOP1.

A subset of ATA mAbs recognize TOP1 better in complex with DNA

TOP1 can form a covalent complex with DNA, termed TOP1-DNA cleavage complex (TOP1cc)[18]. To study the effect of DNA binding on the recognition of TOP1 by the ATA mAbs, we next compared mAb reactivity towards TOP1 and TOP1cc. TOP1cc was formed using a suicide substrate, a double-stranded DNA ligand which covalently and irreversibly binds to TOP1[21]. This binding results in a size shift which can be visualized by gel electrophoresis (Fig. 2A). By coating of either antigen on an ELISA plate, the recognition of TOP1 and TOP1cc by the ATA mAbs could be compared. ATA mAb 2F8 recognized TOP1 and TOP1cc to a similar extent (Fig. 2B-C). In contrast, ATA mAbs 7G6 and 9D11 recognized TOP1cc with higher relative avidity than TOP1 (Fig. 2B-C). None of the mAbs reacted to suicide substrate alone (Suppl. Fig. S2A). To further substantiate the differential binding of ATA to TOP1 and TOP1cc, we measured the reactivity towards either antigen by IgG in culture supernatants of 13 additional, single-cell sorted TOP1-reactive B cell clones. Only 3 of the 13 clones recognized TOP1 and TOP1cc to a similar extent, whereas the other 10 clones showed enhanced recognition of TOP1cc as compared to TOP1 (Fig. 2D). Importantly, we noted a strong variation between clones as to the extent to which TOP1cc was differentially recognized.

We next analyzed the differential binding under native conditions in solution to exclude that immobilization of either protein to the ELISA plate would have caused the observed effects. We employed mass photometry to determine the binding stoichiometry of the ATA mAbs to TOP1 and TOP1cc. This single particle interferometric scattering microscopy technique allows to analyze the formation of immune complexes in solution formed upon incubation of ATA mAbs with TOP1 and TOP1cc (Fig. 2E, Suppl. Fig. S2B-C, Suppl. Table 1). In the presence of antigen excess, ATA-IgG 2F8 bound both TOP1 and TOP1cc and efficiently formed immune complexes containing two antigens (Fig. 2E). ATA-IgG 7G6 and ATA-IgG 9D11 did not show complete binding to TOP1 (Fig. 2E). In these conditions, antibodies binding no or only one antigen could be detected, especially for ATA-IgG 9D11. In contrast, nearly complete binding of 7G6 and 9D11 was observed to TOP1cc (Fig. 2E). Hence, this independent approach confirmed the finding that certain ATA mAbs differentially recognize TOP1 and TOP1cc.

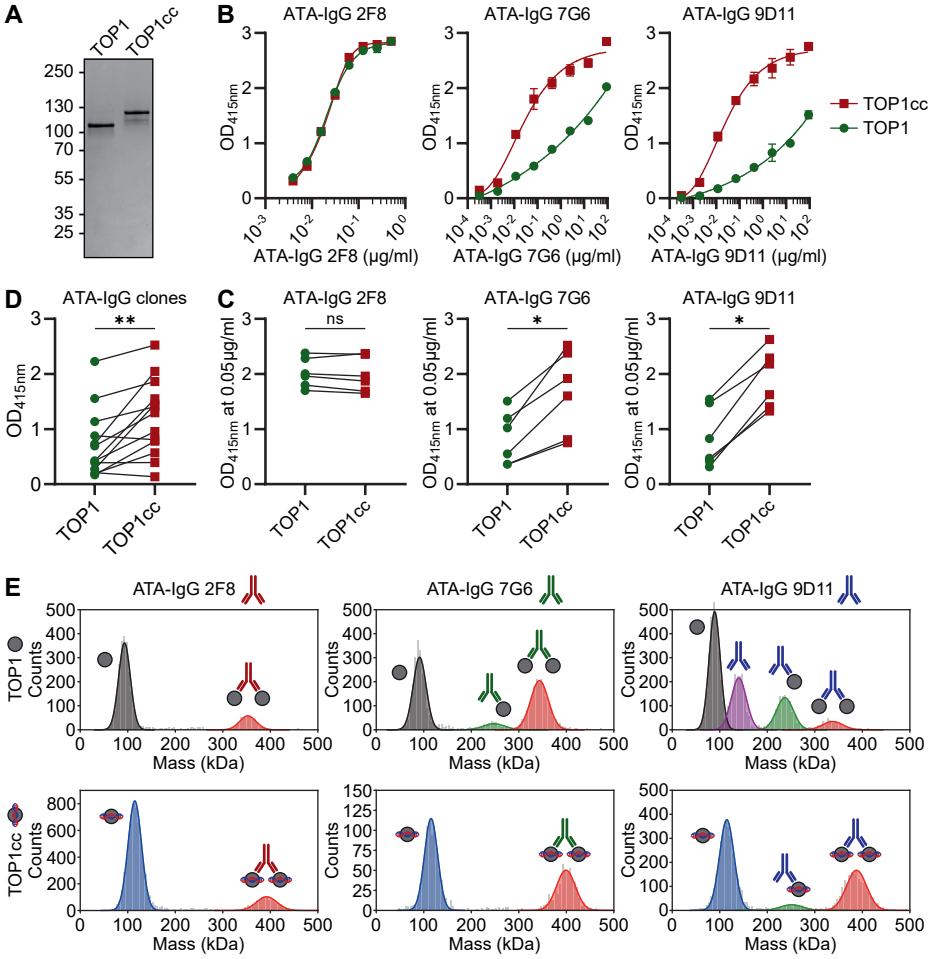

Figure 2. Reactivity of ATA mAbs towards TOP1 and TOP1cc. (A) Gel electrophoresis of TOP1 upon pre-incubation without or with suicide substrate (TOP1 and TOP1cc, respectively) under non-reducing conditions. Molecular weight in kilodaltons (kDa) was estimated using a protein ladder. **(B)** Reactivity of ATA mAbs 2F8, 7G6 and 9D11 towards TOP1 and TOP1cc in an anti-TOP1/TOP1cc-IgG ELISA. Data points represent the mean and standard deviation of two technical replicates from an individual experiment. **(C)** Quantification of the binding of 0.05µg/ml ATA mAbs 2F8, 7G6 and 9D11 to TOP1 and TOP1cc. Data is derived from six independent experiments. **(D)** Reactivity towards TOP1 and TOP1cc by IgG in cultures supernatants (n=13) of single-cell sorted CD19^{+} TOP1$^{+/+}$ B cells with verified reactivity towards TOP1. **(E)** Representative mass histograms of ATA mAbs incubated with an excess of TOP1 and TOP1cc as obtained by mass photometry. Data is representative of two independent experiments. An overview of detected masses can be found in Suppl. Table 1. **(B-D)** Optical density was measured at 415 nanometers (OD_{415nm}). **(C-D)** Wilcoxon matched-pairs signed rank test was used to test for significant differences. ns = not significant, * = p<0.05, ** = p<0.005, *** = p<0.001.

Polyclonal IgG autoantibodies from ATA^{+} SSc patients differentially recognize TOP1cc

Differential recognition of TOP1/TOP1cc by ATA-IgG could affect the functionality of ATAs and, hence, influence disease pathogenesis. Therefore, we next assessed differential recognition of TOP1/TOP1cc by polyclonal ATA in the circulation of ATA^{+} SSc patients.

Half-maximal binding titers of polyclonal IgG to TOP1 and TOP1cc were determined by serial dilutions of patient plasma (Fig. 3A). ATA mAbs were taken along in these assays to control for comparable coating concentrations of TOP1 and TOP1cc (ATA mAb 2F8), and as positive controls for the differential recognition of TOP1cc compared to TOP1 (ATA mAbs 7G6 and 9D11). Plasma of all ATA$^+$ SSc patients (n=21) showed higher IgG titers to TOP1cc compared to TOP1 (Fig. 3B). Patients varied as to the extent of differential TOP1/TOP1cc recognition. The difference between anti-TOP1-IgG and anti-TOP1cc-IgG titers was modest for some patients. For others, much higher dilutions of plasma were needed to reach the same binding signal for TOP1cc in comparison to TOP1 (up to 30.000 difference in dilution factor) (Fig. 3C). Again, we excluded suicide substrate recognition as confounder, as binding to suicide substrate was minimal to undetectable (Suppl. Fig. S3A). Also, plasma from ACA$^+$ SSc patients and healthy donors generated signals below the limit of detection (Suppl. Fig. S3B). Together, these findings indicate that enhanced TOP1cc recognition by a subset of ATAs is a feature commonly present in ATA$^+$ SSc patients.

To explore the possible clinical relevance of our finding, we assessed the relation between the differential recognition of TOP1cc and clinical disease parameters using the absolute

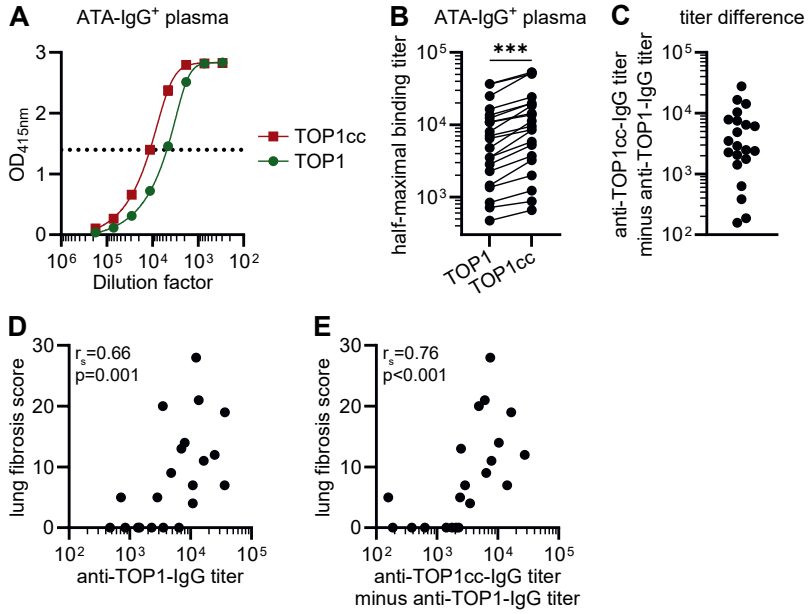

Figure 3. Reactivity of IgG in ATA-IgG$^+$ plasma towards TOP1 and TOP1cc. (A) Binding of IgG in plasma of an ATA$^+$ SSc patient to TOP1 and TOP1cc in an anti-TOP1/TOP1cc-IgG ELISA. Optical density was measured at 415 nanometers (OD_{415nm}). Dotted line represents an OD_{415nm} of 1.4 which was considered the half-maximal signal of the assay. **(B)** Anti-TOP1/TOP1cc-IgG expressed as half-maximal binding titers (interpolated dilution generating an optical density of 1.4 at 415 nanometers) in plasma of ATA$^+$ SSc patients (n=21). Half-maximal binding titers were statistically compared using the Wilcoxon matched-pairs signed rank test. ns = not significant, * = p<0.05, ** = p<0.005, *** = p<0.001. **(C)** Difference between anti-TOP1cc-IgG titer and anti-TOP1-IgG titer in plasma of ATA$^+$ SSc patients. **(D-E)** Correlation between the lung fibrosis score and the anti-TOP1-IgG titer **(D)** and the difference between anti-TOP1cc-IgG and anti-TOP1-IgG titer **(E)**. Correlations are described using the Spearman's rank correlation coefficient (r_s).

difference between anti-TOP1cc-IgG and anti-TOP1-IgG titers (anti-TOP1cc-IgG titer minus anti-TOP1-IgG titer) as read-out. This difference correlated with anti-TOP1-IgG titers (r_s=0.91) (Suppl. Fig. S3C). In addition, both the anti-TOP1-IgG titer and the difference between anti-TOP1cc-IgG and anti-TOP1-IgG titers correlated with the lung fibrosis score (r_s=0.65 and r_s=0.76, respectively) (Fig. 3D-E). Similar trends were observed for the modified Rodnan skin score (Suppl. Fig. S3D-E). Together, the data indicate that anti-TOP1-IgG titers and anti-TOP1cc-IgG titers are strongly related and correlate with clinical disease.

Anti-TOP1cc autoantibodies are predominantly present in the IgG1 and IgM compartment
Isotype and subclass usage strongly affects antibody effector functions and provides insights into the underlying B cell response[23,24]. Therefore, we studied the recognition of TOP1 and TOP1cc by antibodies of various subclasses and isotypes in plasma of ATA$^+$ SSc patients. Presence of ATA among the IgG subclasses was variable, as IgG1, IgG2, IgG3 and IgG4 anti-TOP1-autoantibodies could be detected in 67%, 81%, 52% and 95% of the samples (n=21), respectively (Suppl. Fig. S4A-D). Therefore, we limited the analysis to samples in which TOP1 was recognized by multiple IgG subclasses (n=8 for IgG1/3/4, n=7

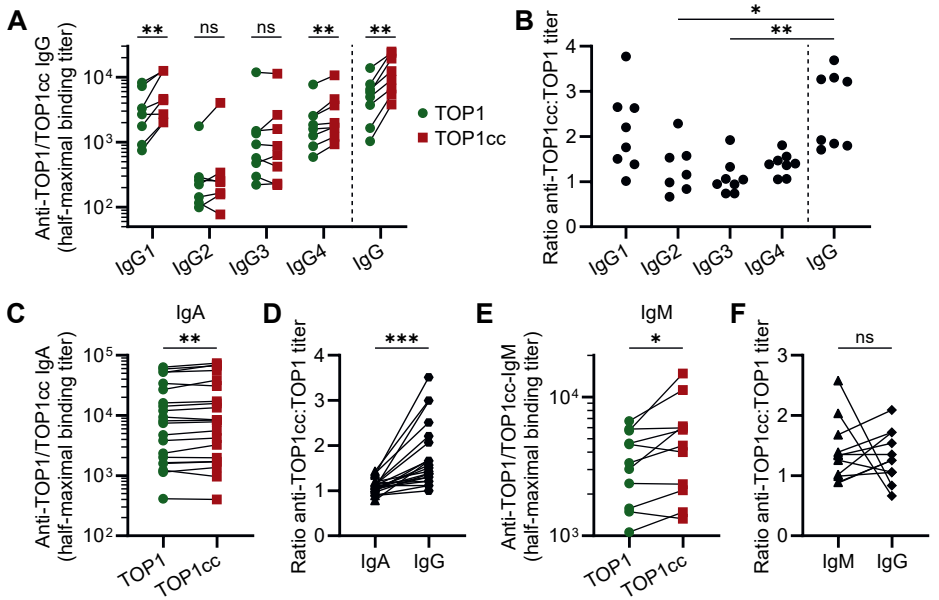

Figure 4. Reactivity towards TOP1 and TOP1cc by IgG subclasses, IgA and IgM in plasma of ATA$^+$ SSc patients. (A) Half-maximal binding titers of IgG1-4 and total IgG in plasma of ATA-IgG$^+$ SSc patients (n=8 for IgG1, 3, 4, n=7 for IgG2) to TOP1 and TOP1cc. **(B)** Ratio between anti-TOP1cc and anti-TOP1 titers of IgG1-4 and total IgG in plasma. Ratios of IgG1-4 were compared to total IgG using the Kruskal-Wallis test combined with Dunn's multiple comparison. **(C)** Reactivity of IgA in plasma of ATA-IgG$^+$ SSc patients (n=21) towards TOP1 and TOP1cc. **(D)** Anti-TOP1cc-IgA/G titers expressed as ratio to anti-TOP1-IgA/G titers. **(E)** Reactivity of IgM in plasma of ATA-IgM$^+$ SSc patients (n=11) towards TOP1 and TOP1cc. **(F)** Anti-TOP1cc-IgM/IgG titers expressed as ratio to anti-TOP1-IgA/G titers. **(A, C, E)** Binding to TOP1 and TOP1cc is expressed as half-maximal binding titer, the interpolated dilution generating an optical density of 1.4 at 415 nanometers. **(C-E)** Half-maximal binding titers to TOP1 and TOP1cc were statistically compared using the Wilcoxon matched-pairs signed rank test. **(D, F)** Ratio titers were compared using the Mann-Whitney U test. **(A-F)** ns = not significant, * = p<0.05, ** = p<0.005, *** = p<0.001.

for IgG2) and in which total IgG recognized TOP1cc better than TOP1 (Fig. 4A). Enhanced recognition of TOP1cc compared to TOP1 was observed for IgG1 and IgG4, but not for IgG2 and IgG3 (Fig. 4A). To compare the relative difference in TOP1cc binding by the IgG subclasses to total IgG, anti-TOP1cc titers were normalized to anti-TOP1 titers by expressing the titers as a ratio (anti-TOP1cc titer divided by anti-TOP1 titer). The relative difference in TOP1cc binding by IgG1 was comparable to total IgG, while the ratio between anti-TOP1cc and anti-TOP1 titers for IgG2-4 were lower (Fig. 4B). Consequently, the differential recognition of TOP1 upon DNA binding appears most prominent for IgG1.

TOP1-reactive antibodies of the IgA isotype can be detected in almost all ATA-IgG$^+$ SSc patients[8]. Accordingly, we detected anti-TOP1-IgA in all ATA-IgG$^+$ SSc patients (n=21) included in this study (Fig. 4C). These IgA antibodies recognized TOP1cc slightly better in comparison to TOP1 (Fig. 4C). However, the relative difference in the half-maximal binding titers between TOP1 and TOP1cc was significantly higher in the IgG compartment (Fig. 4D).

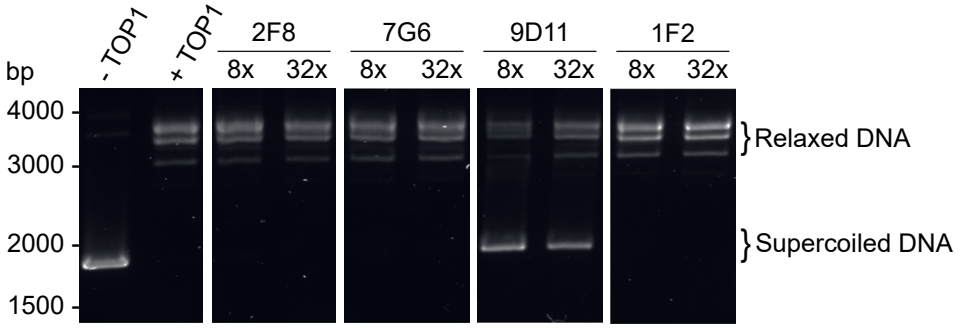

Figure 5. Effect of ATA mAbs on the enzymatic function of TOP1. DNA relaxation assay with TOP1 upon pre-incubation with an 8x and 32x molar equivalent of the ATA mAbs. A monoclonal antibody reactive towards citrullinated proteins (1F2) was used as negative control. DNA was visualized with a fluorescent DNA stain. Molecular weight of DNA in base pairs (bp) was estimated using a DNA ladder. Data are representative of two independent experiments.

For IgM, we observed that only 2 out of 21 ATA-IgG$^+$ patients generated higher signals on the anti-TOP1-IgM ELISA compared to controls (Suppl. Fig. S4E-G). To prevent interference of aspecific antibodies in the assay, we compared the reactivity of IgM antibodies towards TOP1 and TOP1cc in the two ATA-IgM$^+$ SSc patients and selected 9 other samples of ATA$^+$ SSc patients with high levels of ATA-IgM from a previous study (Suppl. Fig. S4H, Table 1)[8]. TOP1cc was better recognized than TOP1 by IgM antibodies in these samples (Fig. 4E). The relative difference in the half-maximal binding titers to TOP1 and TOP1cc was comparable between IgG and IgM (Fig. 4F). Together, these data indicate that the differential recognition of TOP1 and TOP1cc is predominantly found in the IgM compartment and in the IgG1 subclass.

ATA mAb can inhibit the enzymatic function of TOP1

We further characterized the ATA mAbs by assessing their effect on the enzymatic function of TOP1. Previous work showed that purified immunoglobulins from ATA$^+$ SSc

patients can inhibit the enzymatic function of TOP1[25,26]. The enzymatic activity of TOP1 can be measured based on the relaxation of supercoiled plasmid DNA which impairs the mobility of DNA through agarose gels (Fig. 5). Pre-incubation of TOP1 with ATA-IgG 2F8, ATA-IgG 7G6 and a control mAb did not affect the enzymatic function of TOP1 (Fig. 5). In contrast, supercoiled plasmid DNA was still apparent in the condition in which TOP1 was pre-incubated with ATA mAb 9D11 (Fig. 5). This indicates that ATA mAb 9D11 can inhibit the enzymatic function of TOP1.

Enhanced induction of cytokine production by anti-TOP1cc mAbs in complex with TOP1cc
The enhanced binding of ATA mAbs to TOP1cc compared to TOP1 may have functional implications on the immunostimulatory capacity of ATAs. Therefore, we stimulated the monocytic THP-1 cell line with ATA mAbs complexed with plate-bound TOP1 and TOP1cc and subsequently determined the secretion of IL-8. Minimal secretion of IL-8 by THP-1 cells was detected in conditions with TOP1 and TOP1cc coating to which no antibody or a negative control antibody was added (Fig. 6, Suppl. Fig. S5). The ATA mAb 2F8, which binds to TOP1 and TOP1cc to a similar extent, induced comparable levels of IL-8 if complexed with TOP1cc or TOP1 (Fig. 6, Suppl. Fig. S5). In contrast, ATA-mAbs 7G6 and 9D11, which both bind TOP1cc better than TOP1, induced higher production of IL-8 by THP-1 when complexed with TOP1cc compared to TOP1 (Fig. 6, Suppl. Fig. S5). These data show functionality of the ATA mAbs generated and indicate that the ability of ATA to induce inflammation can be affected by the binding of TOP1 to DNA.

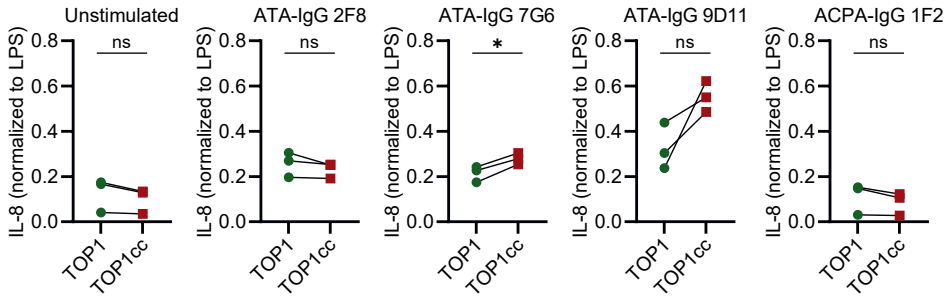

Figure 6. IL-8 production by THP-1 cells stimulated with ATA mAbs in complex with TOP1 and TOP1cc. Normalized levels of IL-8 in culture supernatants of THP-1 cells stimulated for 24 hours with ATA mAbs in complex with plate-bound TOP1 and TOP1cc. Conditions to which no mAb or the ACPA-IgG mAb 1F2 was added were used as negative controls. IL-8 levels were normalized to the levels of IL-8 detected in culture supernatant of THP-1 cells stimulated with 1µg/ml lipopolysaccharide (LPS). Data is obtained from three independent experiments which are connected by lines.

Discussion

Predictability of disease progression forms a major challenge in the clinical management of SSc due to heterogeneity in clinical presentation and course of disease. To gain insights into the molecular mechanisms driving the disease, we here focused on the ATA B cell response and assessed whether DNA binding by TOP1 would affect its recognition by ATAs. By studying monoclonal and polyclonal ATAs, we observed remarkable heterogeneity among these autoantibodies in the recognition of TOP1 and TOP1cc. In fact, a subset of ATAs recognized TOP1cc better than TOP1, indicating that TOP1cc formation induces

conformational changes, presumably, that enhance the antigenic properties of individual TOP1 epitopes and, consequently, the immunostimulatory properties of ATAs.

The differential recognition of TOP1 and TOP1cc by ATAs could relate to disease by various means. We observed that enhanced recognition of TOP1cc can be found in all ATA$^+$ SSc patients, yet increasingly in patients with interstitial lung disease and in those with higher anti-TOP1-IgG levels in serum. Hence, it is likely that TOP1cc functions as an enhancer of the stimulation of ATA$^+$ B cells. In fact, our data indicate that TOP1cc could preferentially stimulate a subset of B cells expressing ATA with enhanced recognition of TOP1cc epitopes.

Stimulation of these cells may be further amplified by BCR-mediated internalization of DNA in complex with TOP1 and subsequent co-engagement of Toll-like receptor 9 (TLR9)[27–29]. Consequently, TOP1cc recognition may be relevant for both the initial break of B cell tolerance to TOP1 and, likewise, the continuous activation of ATA B cells in established disease. In this context, it is important that we noted the predominant presence of 'TOP1cc-enhanced' ATA within the IgM and the IgG1 subclass compartment. The presence of TOP1cc-enhanced reactivity in the IgM compartment makes the naive B cell compartment susceptible to strong BCR-mediated stimulation, while TLR stimulation synergizes with BCR signaling to induce AID which mediates BCR class-switching[28,30]. Previously, we could show that both the presence of ATA-IgM as well as ATA-IgG levels in serum associated with progressive disease, supporting this concept[8]. In addition, the presence of ATA-secreting cells in the circulation, a sign of recent B cell activation, associated with presence and severity of interstitial lung disease[7]. Together, these results indicate that the formation of TOP1cc could be important for ATA B cell activation and suggest that this process may be relevant to initiate and drive ATA$^+$ disease.

Our findings imply that TOP1 in complex with DNA is the autoantigen primarily targeted by the ATA B cell response. Differential recognition of TOP1 and TOP1cc likely depends on conformational changes that occur when TOP1 binds DNA[31–33]. This conformational change only affects the binding of ATAs that recognize epitopes of TOP1 which are altered and, thus, probably represent a subset of ATA B cells. This is consistent with the finding that ATA mAbs differentially bind to TOP1 and TOP1cc, bind to unique epitopes and vary in their ability to inhibit the enzymatic function of TOP1. Also, our data indicate that such interaction may enhance ATA functional properties inducing or supporting inflammatory processes. The relevance of these functional effects and the context in which the actual antigen is encountered by ATAs and TOP1-reactive B cells remains to be determined, particularly within affected tissues. It has been described that TOP1 isolated from nuclei of SSc skin fibroblasts shows reduced enzymatic activity and is more often modified with a small ubiquitin-like modifier (SUMO)[34]. These traits are associated with the presence of TOP1cc, as TOP1cc is SUMOylated in pathways needed to repair DNA lesions trapped in TOP1cc[35]. Another variable could be the source of DNA incorporated in TOP1cc, as human TOP1 can also bind microbial DNA[36]. Microbial DNA is a more potent inducer of TLR9 signaling in comparison to human DNA, which might further enhance the pro-inflammatory potential of TOP1cc[37]. Together, such variables could determine the immunological properties of TOP1, add to the enhanced stimulation of B cells and indicate the need for molecular analyses of TOP1 in affected tissues.

In conclusion, our data indicate that DNA binding by TOP1, a nuclear autoantigen in SSc, affects the recognition of the antigen by disease-specific autoantibodies. This enhanced antigen binding extends the relevance of the well-appreciated pro-inflammatory effects of nucleic acid binding by nuclear antigens. Modulation of autoantigen recognition by nucleic acid binding could affect autoreactive B cell responses targeting nuclear proteins in SSc and other autoimmune diseases, thereby modulating their disease processes and course.

Acknowledgements
Flow cytometry was performed at the Flow Cytometry Core Facility (FCF) of the Leiden University Medical Center.

Conflict of interest
The authors declare no competing interests related to the work presented in this paper.

Funding sources
Research presented in this paper was funded by the Dutch Arthritis Foundation (LLP5), the IMI funded project RTCure (777357), Health~Holland Life Sciences & Health sector programs Target to B! (LSHM18055-5GF) and Immune HealthSeed (LSHM22042-SFG), a European Research Council Advanced grant (AdG2019-884796, to REMT) and a NWO-ZonMW VIDI grant (09150172010067, to HUS).

Author contributions
Conceptualization: SN, DMHR, AJRH, CMF, JKVB, REMT, HUS. Designing and conducting experiments: SN, CW, DMHR, MJALW. Methodology: SN, CW, DMHR, MJALW, RQK, NL, CMF, REMT, HUS. Formal analysis: SN, DMHR, MJALW, HUS. Data interpretation: SN, DMHR, MJALW, AJRH, CMF, JKVB, REMT, HUS. Supervision: REMT, HUS. Writing original draft: SN, HUS. Revision of the manuscript and approval of the final version for submission: all authors.

Data availability statement
Data presented in this paper are available upon reasonable request.

References

1 Pope, J. E. *et al*. State-of-the-art evidence in the treatment of systemic sclerosis. *Nat Rev Rheumatol* **19**, 212–226 (2023).
2 Pisetsky, D. S. Unique interplay between antinuclear antibodies and nuclear molecules in the pathogenesis of systemic lupus erythematosus. *Arthritis Rheumatol* **76**, 1334–1343 (2024).
3 Liem, S. I. E. *et al*. Autoreactive B cell responses targeting nuclear antigens in systemic sclerosis: Implications for disease pathogenesis. *Semin Arthritis Rheum* **58**, 152136 (2023).
4 Pokeerbux, M. R. *et al*. Survival and prognosis factors in systemic sclerosis: data of a French multicenter cohort, systematic review, and meta-analysis of the literature. *Arthritis Res Ther* **21**, 86 (2019).
5 Bournia, V. K. *et al*. All-cause mortality in systemic rheumatic diseases under treatment compared with the general population, 2015-2019. *RMD Open* **7**, e001694 (2021).
6 Nihtyanova, S. I. & Denton, C. P. Autoantibodies as predictive tools in systemic sclerosis. *Nat Rev Rheumatol* **6**, 112–116 (2010).
7 Wortel, C. M. *et al*. Anti-topoisomerase, but not anti-centromere B cell responses in systemic sclerosis display active, Ig-secreting cells associated with lung fibrosis. *RMD Open* **9**, e003148 (2023).
8 Boonstra, M. *et al*. Association of anti–topoisomerase I antibodies of the IgM isotype with disease progression in anti–topoisomerase I–positive systemic sclerosis. *Arthritis Rheumatol* **72**, 1897–1904 (2020).
9 Bergmann, C. *et al*. Treatment of a patient with severe systemic sclerosis (SSc) using CD19-targeted CAR T cells. *Ann Rheum Dis* **82**, 1117–1120 (2023).
10 Goswami, R. P. *et al*. Rituximab in the treatment of systemic sclerosis-related interstitial lung disease: a systematic review and meta-analysis. *Rheumatology (Oxford)* **60**, 557–567 (2021).
11 Arcand, J., Robitaille, G., Koenig, M., Senécal, J. L. & Raymond, Y. Heparin inhibits the interaction of DNA topoisomerase I/anti–topoisomerase I immune complexes with heparan sulfate on dermal fibroblasts. *Arthritis Rheum* **64**, 1632–1641 (2012).
12 Hénault, J., Robitaille, G., Senécal, J. L. & Raymond, Y. DNA topoisomerase I binding to fibroblasts induces monocyte adhesion and activation in the presence of anti–topoisomerase I autoantibodies from systemic sclerosis patients. *Arthritis Rheum* **54**, 963–973 (2006).
13 Hénault, J., Tremblay, M., Clément, I., Raymond, Y. & Senécal, J. L. Direct binding of anti–DNA topoisomerase I autoantibodies to the cell surface of fibroblasts in patients with systemic sclerosis. *Arthritis Rheum* **50**, 3265–3274 (2004).
14 Rubin, S. J. S., Bloom, M. S. & Robinson, W. H. B cell checkpoints in autoimmune rheumatic diseases. *Nat Rev Rheumatol* **15**, 303–315 (2019).
15 Kwak, K., Akkaya, M. & Pierce, S. K. B cell signaling in context. *Nat Immunol* **20**, 963–969 (2019).
16 Suurmond, J. & Diamond, B. Autoantibodies in systemic autoimmune diseases: specificity and pathogenicity. *J Clin Invest* **125**, 2194–2202 (2015).
17 Kringelum, J. V., Nielsen, M., Padkjær, S. B. & Lund, O. Structural analysis of B-cell epitopes in antibody:protein complexes. *Mol Immunol* **53**, 24–34 (2013).
18 Pommier, Y., Sun, Y., Huang, S. Y. N. & Nitiss, J. L. Roles of eukaryotic topoisomerases in transcription, replication and genomic stability. *Nat Rev Mol Cell Biol* **17**, 703–721 (2016).
19 Sordet, O. *et al*. Topoisomerase I requirement for death receptor-induced apoptotic nuclear fission. *J Biol Chem* **283**, 23200–23208 (2008).
20 Meijs, J. *et al*. Therapeutic and diagnostic outcomes of a standardised, comprehensive care pathway for patients with systemic sclerosis. *RMD Open* **2**, e000159 (2016).
21 Kristoffersen, E. L. *et al*. Real-time investigation of human topoisomerase I reaction kinetics using an optical sensor: a fast method for drug screening and determination of active enzyme concentrations. *Nanoscale* **7**, 9825–9834 (2015).
22 Kissel, T. *et al*. Antibodies and B cells recognising citrullinated proteins display a broad cross-reactivity towards other post-translational modifications. *Ann Rheum Dis* **79**, 472–480 (2020).

23 Lu, L. L., Suscovich, T. J., Fortune, S. M. & Alter, G. Beyond binding: antibody effector functions in infectious diseases. *Nat Rev Immunol* **18**, 46–61 (2017).
24 Volkov, M. *et al*. Comprehensive overview of autoantibody isotype and subclass distribution. *J Allergy Clin Immunol* **150**, 999–1010 (2022).
25 Bankamp, L. *et al*. Functional autoantibodies in systemic sclerosis: influence of autologous stem cell transplantation and correlation with clinical outcome. *Rheumatology (Oxford)* **62**, 2168–2177 (2023).
26 Scott Samuels, D., Tojo, T., Homma, M. & Shimizu, N. Inhibition of topoisomerase I by antibodies in sera from scleroderma patients. *FEBS Lett* **209**, 231–234 (1986).
27 Eckl-Dorna, J. & Batista, F. D. BCR-mediated uptake of antigen linked to TLR9 ligand stimulates B-cell proliferation and antigen-specific plasma cell formation. *Blood* **113**, 3969–3977 (2009).
28 Pone, E. J. *et al*. BCR-signalling synergizes with TLR-signalling for induction of AID and immunoglobulin class-switching through the non-canonical NF-κB pathway. *Nat Commun* **3**, 767 (2012).
29 Viglianti, G. A. *et al*. Activation of autoreactive B cells by CpG dsDNA. *Immunity* **19**, 837–847 (2003).
30 Pone, E. J. *et al*. B cell TLR1/2, TLR4, TLR7 and TLR9 interact in induction of class switch DNA recombination: Modulation by BCR and CD40, and relevance to T-independent antibody responses. *Autoimmunity* **48**, 1–12 (2015).
31 Carey, J. F., Schultz, S. J., Sisson, L., Fazzio, T. G. & Champoux, J. J. DNA relaxation by human topoisomerase I occurs in the closed clamp conformation of the protein. *PNAS* **100**, 5640–5645 (2003).
32 Takahashi, D. T. *et al*. Topoisomerase I (TOP1) dynamics: conformational transition from open to closed states. *Nat Commun* **13**, 59 (2022).
33 Woo, M. H. *et al*. Locking the DNA topoisomerase I protein clamp inhibits DNA rotation and induces cell lethality. *PNAS* **100**, 13767–13772 (2003).
34 Zhou, X. *et al*. Decreased catalytic function with altered sumoylation of DNA topoisomerase I in the nuclei of scleroderma fibroblasts. *Arthritis Res Ther* **13**, R128 (2011).
35 Sun, Y. *et al*. A conserved SUMO pathway repairs topoisomerase DNA-protein cross-links by engaging ubiquitin-mediated proteasomal degradation. *Sci Adv* **6**, 6290–6303 (2020).
36 Nitiss, J. L., Kiianitsa, K., Sun, Y., Nitiss, K. C. & Maizels, N. Topoisomerase Assays. *Curr Protoc* **1**, e250 (2021).
37 Lande, R. *et al*. Plasmacytoid dendritic cells sense self-DNA coupled with antimicrobial peptide. *Nature* **449**, 564–569 (2007).

Supplementary Figures

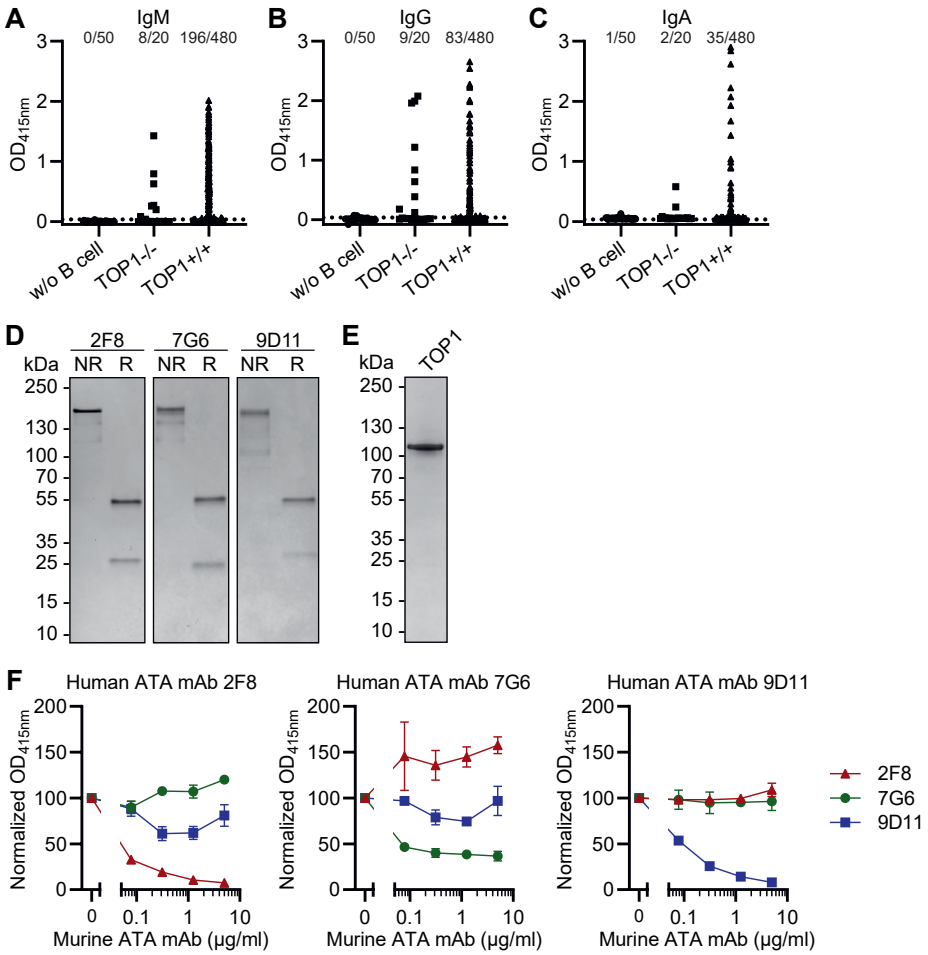

Supplementary Figure S1. Generation and characterization of patient-derived ATA mAbs. (A-C) Presence of IgM **(A)**, IgG **(B)** and IgA **(C)** in the culture supernatant of 480 single-cell sorted TOP1$^{+/+}$ B cells. Culture supernatants of 20 B cells lacking reactivity towards TOP1 (TOP1$^{-/-}$) and 50 culture supernatants without B cells (w/o B cell) were taken along as controls. Cut-off (mean of TOP1$^{-/-}$ B cells + 4x standard devation) is represented by the dotted line. Numbers indicate the amount of positive wells. **(D-E)** Gel electrophoresis of ATA mAbs under non-reducing (NR) and reducing (R) conditions **(D)** and of TOP1 under non-reducing conditions **(E)**. Molecular weight in kilodaltons (kDa) was estimated using a protein ladder. **(F)** Binding of patient-derived ATA mAbs 2F8 **(I)**, 7G6 **(J)** and 9D11 **(K)** with a human constant domain (human ATA mAbs) to TOP1-coated ELISA plates preincubated with ATA mAbs with a murine constant domain (murine ATA mAbs). Binding was normalized to the signal obtained when no murine mAb was added. Concentrations of human mAbs were in the linear range of the ATA-IgG ELISA; 2F8 - 0.04µg/ml, 7G6 & 9D11 - 1µg/ml. Data is representative of three independent experiments and each data point represents the mean and standard devation of two technical replicates from an individual experiment. **(A-C, F)** Optical density was measured at 415 nanometers (OD_{415nm}).

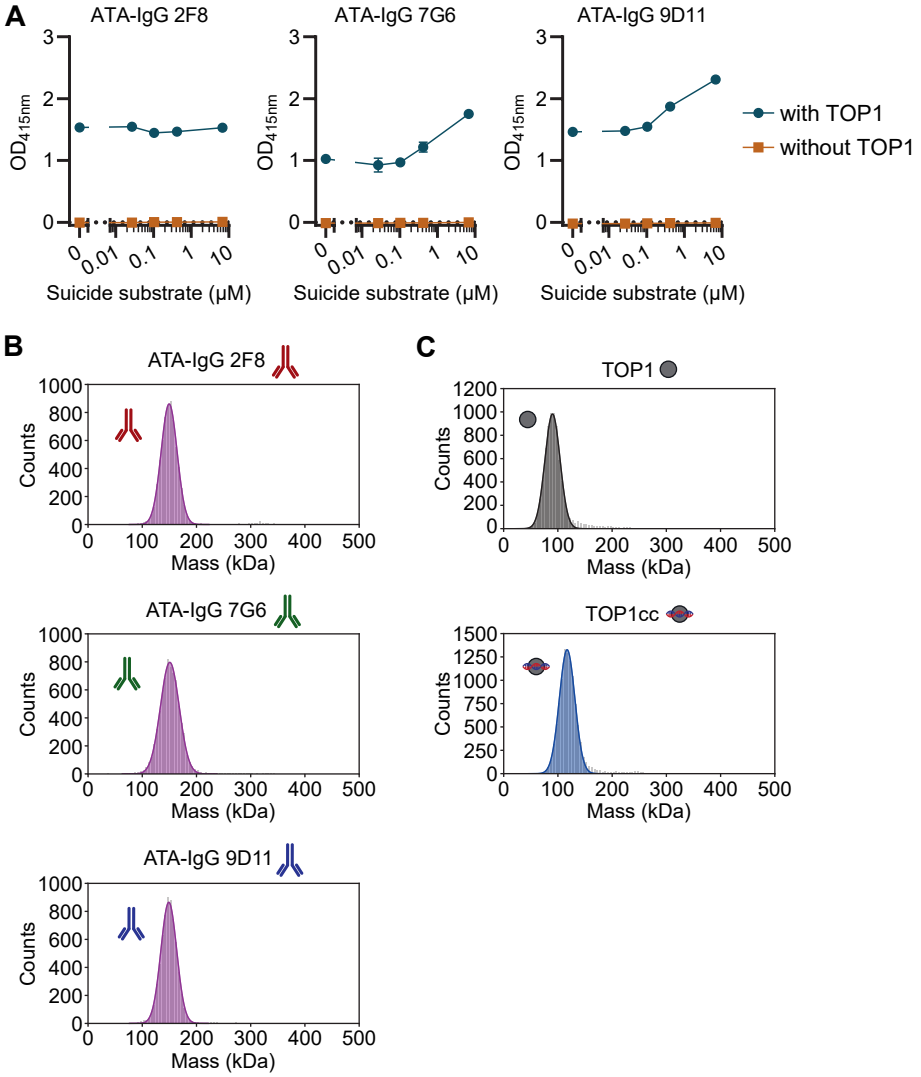

Supplementary Figure S2. Validation of assays used to measure the reactivity of ATA mAbs towards TOP1 and TOP1cc by ELISA and mass photometry. (A) Binding of the ATA mAbs in an ELISA coated with and without TOP1 upon preincubation with a concentration range of suicide substrate. Concentrations of human mAbs were in the linear range of the ELISA; 0.08μg/ml of ATA-IgG 2F8, 9μg/ml of ATA-IgG 7G6 and 2.5μg/ml of ATA-IgG 9D11. Optical density was measured at 415 nanometers (OD_{415nm}). **(B-C)** Representative mass histograms of the ATA mAbs **(B)**, TOP1 and TOP1cc **(C)** as obtained by mass photometry. An overview of detected masses can be found in Suppl. Table 1.

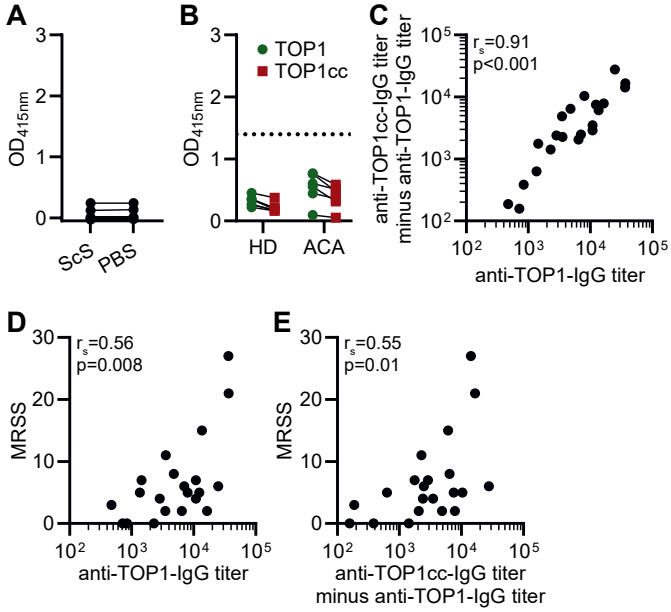

Supplementary Figure S3. Relation between the recognition of TOP1 and TOP1cc and clinical disease. **(A)** Reactivity of IgG in plasma of ATA$^+$ SSc patients (n=21) towards suicide substrate (ScS) and PBS (negative control). Signal was determined at the plasma concentration generating the half-maximal binding titer to TOP1 of the corresponding patient. **(B)** Reactivity of IgG in plasma of healthy donors (HD) (n=6) and ACA$^+$ SSc patients (n=6) towards TOP1 and TOP1cc. Samples were diluted 625x, matching the lowest anti-TOP1-IgG half-maximal binding titers in a cohort of 21 ATA-IgG$^+$ SSc patients. Half-maximal binding titer is represented by the dotted line (OD=1.4). **(C)** Correlation between anti-TOP1-IgG titer and difference between anti-TOP1cc-IgG and anti-TOP1-IgG titer (anti-TOP1cc-IgG titer minus anti-TOP1-IgG titer) in 21 ATA-IgG$^+$ SSc patients. **(D-E)** Correlation between the modified Rodnan skin score (MRSS) and the anti-TOP1-IgG titer **(H)** and the difference between anti-TOP1cc-IgG and anti-TOP1-IgG titer. **(A-B)** Binding was based on optical density measured at 415 nanometers (OD_{415nm}). **(C-E)** Correlations are described using the Spearman's rank correlation coefficient (r_s).

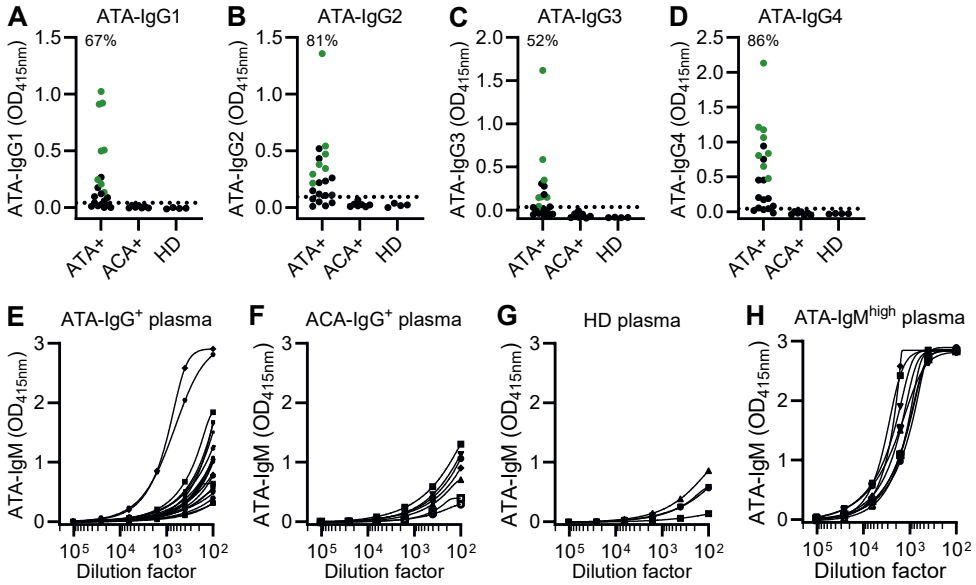

Supplementary Figure S4. Binding of TOP1 by IgG subclasses and IgM in plasma of ATA⁺ SSc patients. (A-D) Reactivity of IgG1-4 in plasma of ATA⁺ SSc patients (n=21), ACA⁺ SSc patients (n=7) and healthy donors (HD) (n=4) towards TOP1. Plasma samples were diluted 8000x for IgG1, 1000x for IgG2, 10000x for IgG3 and 3200x for IgG4. Cut-off (mean of ACA⁺ SSc patients and HD's + 4x standard deviation) is represented by the dotted line. Frequency of positive samples are indicated in percentages. Selected samples used to analyze the reactivity of IgG subclasses towards TOP1 and TOP1cc are indicated in green. **(E-H)** Binding of TOP1 by IgM in serial diluted plasma of ATA⁺ SSc patients (n=21) **(E)**, ACA-IgG⁺ patients (n=7) **(F)**, healthy donors (HD) (n=4) **(G)** and ATA-IgM^{high} patients **(H)**. **(A-H)** Optical density was measured at 415 nanometers (OD_{415nm}).

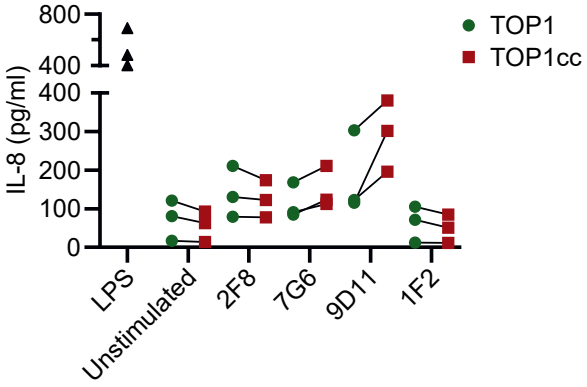

Supplementary Figure S5. IL-8 concentration in culture supernatant of THP-1 cells stimulated with ATA mAbs in complex with plate-bound TOP1 and TOP1cc. IL-8 levels in culture supernatants of THP-1 cells stimulated for 24 hours with ATA mAbs in complex with plate-bound TOP1 and TOP1cc. Culture supernatants of THP-1 cells stimulated with 1µg/ml LPS were used as positive control. Conditions to which no mAb or ACPA-IgG mAb 1F2 was added were used as negative controls. Data is obtained from three independent experiments which are connected by lines.

Supplementary Table

Supplementary Table S1. Overview of experimental masses determined by mass photometry.

Sample	Species	Experimental mass (kDa)	Confidence interval (standard deviation)	Theoretical mass (kDa)
TOP1	TOP1	90	13	91
TOP1cc	TOP1cc	116	14	119
ATA-IgG 2F8	mAb	149	14	144
ATA-IgG 7G6	mAb	150	17	145
ATA-IgG 9D11	mAb	148	14	145
ATA-IgG 2F8 + TOP1	TOP1	93	12	91
	mAb + 2x TOP1	352	17	326
ATA-IgG 2F8 + TOP1cc	TOP1cc	114	14	119
	mAb + 2x TOP1cc	392	21	382
ATA-IgG 7G6 + TOP1	TOP1	91	13	91
	mAb + 1x TOP1	247	22	236
	mAb + 2x TOP1	343	18	327
ATA-IgG 7G6 + TOP1cc	TOP1cc	115	13	119
	mAb + 2x TOP1cc	399	19	383
ATA-IgG 9D11 + TOP1	TOP1	89	11	91
	mAb	140	15	145
	mAb + 1x TOP1	237	17	236
	mAb + 2x TOP1	337	21	327
ATA-IgG 9D11 + TOP1cc	TOP1cc	114	15	119
	mAb + 1x TOP1cc	250	23	264
	mAb + 2x TOP1cc	387	21	383

Supplementary methods

Recombinant production and purification of TOP1

Human TOP1 was recombinantly produced in insect cells (Protein Facility, Leiden University Medical Center) using an adapted Bac-to-Bac protocol (Invitrogen). In short, a pFastBacHT-A plasmid (OHu27246C, Genscript) encoding the full-length human TOP1 sequence with a N-terminal polyhistidine tag (6x histidine) and tobacco etch virus (TEV) protease recognition site (ENLYFQG) was commercially obtained and transformed into EmBACy competent cells (Geneva Biotech) to generate a recombinant bacmid. The recombinant bacmid was extracted from EmBACy cells by isopropanol precipitation and was subsequently used to transfect sedentary Sf9 insect cells (ThermoFisher). Upon culturing the transfected Sf9 cells for 72 hours at 28°C, culture supernatant containing baculovirus (P0) was collected. The baculovirus-containing supernatant was used to transduce suspension Sf9 cells to recombinantly express human TOP1 and create a baculovirus stock (P1). After culturing the cells for 72 hours at 28°C, transduced Sf9 cells were harvested and resuspended in His-buffer (50 mM HEPES pH7.5, 500 mM NaCl, 1% glycerol and 20 mM imidazole). Cells were lysed using sonication and TOP1 was purified using a HisTrap HP column (Cytiva), using a linear gradient of His-buffer supplemented with 500mM imidazole. Protein fractions were pooled and treated with TEV protease (Protein Facility, Leiden University Medical Center) under overnight dialysis against 20mM HEPES (pH=7.5), 200mM NaCl, 1mM EDTA and 1mM DTT. TOP1 was further purified by cation exchange chromatography (HiTrap SP FF, Cytiva) using a gradient between buffer A (20mM HEPES (pH=7.5), 50mM NaCl, 1mM EDTA and 1mM DTT) and buffer B (buffer A supplemented with 1M NaCl). Purity, integrity and antigenicity of recombinantly-produced TOP1 was validated by ELISA and gel electrophoresis using commercial TOP1 (ProSpec) as comparator.

Generation of patient-derived anti-topoisomerase 1 monoclonal antibodies (ATA mAbs)

ATA mAbs were generated based on the B cell receptor (BCR) sequence of TOP1-reactive B cells obtained from an ATA$^+$ SSc patient. To this end, peripheral blood mononuclear cells (PBMCs) were isolated by Ficoll-Paque gradient centrifugation. PBMCs were stained with LIVE/DEAD™ Fixable Aqua (Invitrogen), anti-CD3 BV510 (UCHT1, BioLegend), anti-CD14 BV510 (M5E2, BioLegend), anti-CD19 APC-Cy7 (SJ25C1, BD Biosciences), anti-CD20 FITC (2H7, BioLegend), anti-CD27 BV421 (M-T271, BD Biosciences) and TOP1 (Prospec) which was conjugated to PE (LNK021RPE, Biorad) and Alexa Fluor™ 647 (A20006, Invitrogen) following the manufacturer's instructions. B cells binding to TOP1-PE and TOP1-Alexa Fluor™ 647 were single-cell sorted with an FACS Aria III 4L (BD Biosciences) and subsequently cultured for 12 days as described previously[1]. Upon culturing, supernatants were harvested to analyze the antibodies secreted by the single-cell sorted B cells and cells were stored in Trizol (ThermoFisher Scientific) for BCR sequencing.

To determine whether secreted antibody was present in the culture supernatants of the single-cell cultured B cells, a total IgM, IgG and IgA ELISA was performed. High binding 384-well Microplates (Corning) were coated with 10µg/ml goat anti-human IgM, IgG or IgM (respectively A80-100, A80-104 and A80-102A, Bethyl Laboratories). Plates were blocked and supernatants were applied in a two-fold dilution. IgM, IgG and IgA were detected with 20ng/µl goat anti-human IgM-HRP, 50ng/ml goat anti-human IgG-HRP or

50ng/ml anti-human IgA-HRP (respectively A80-100P, A80-104P and A80-102P, Bethyl Laboratories). ABTS was used as substrate and plates were measured with a Spectramax I3x Multi-Mode Microplate Reader (Molecular Devices) using SoftMax® Pro 7 (version 7.0.2, Molecular Devices).

To determine the reactivity of the secreted antibodies to human TOP1, ATA-Ig, ATA-IgG and ATA-IgA ELISAs were performed. High binding 384-well Microplates (Corning) were coated with 2.5µg/ml human TOP1 in PBS (pH=8). Plates were blocked and culture supernatants were applied in a two-fold dilution. Ig, IgG and IgA was detected with goat anti-human Ig-HRP (A80-152P, Bethyl Laboratories), rabbit anti-human IgG-HRP (P0214, Dako) and goat anti-human IgA-HRP (A18781, Novex), respectively. ABTS was used as substrate and plates were measured with a Spectramax I3x Multi-Mode Microplate Reader (Molecular Devices) using SoftMax® Pro 7 (version 7.0.2, Molecular Devices).

The variable domain of the BCR of single cell sorted B cells which secreted human TOP1-reactive antibodies in culture were sequenced as described in detail previously[1]. In short, cells were lysed in Trizol and RNA was isolated. cDNA was generated from isolated RNA and used to perform the Anchoring Reverse Transcription of Immunoglobulin Sequences and Amplification by Nested (ARTISAN) PCR[2]. PCR products were sent for Sanger sequencing (Macrogen Europe) and BCR sequences were subsequently determined using IMGT-V-quest[3].

Based on the variable domain of the BCR sequences, plasmids were generated to recombinantly produce ATA mAbs. To this end, constructs containing the sequence encoding the variable domain of the ATA clones and a leader sequence were codon optimized (GeneArt, ThermoFisher Scientific) and ordered with the Kozak sequence (IDT DNA). These constructs were cloned into a pcDNA3.1 (+) expression vector (InVitrogen) using the In-Fusion® Cloning Kit (Takara Bio). To generate mAbs with human constant domains, constructs encoding heavy chain variable domains were cloned into a vector encoding the human IGHG1*03 constant region (P01857, UniProt) and constructs encoding light chain variable domains were cloned into a vector encoding the human IGLC3 or IGKC constant region (in accordance with the light chain of the original BCR; respectively P0DOY3 and P01834, UniProt). To generate mAbs with murine constant domains, constructs were cloned into vectors containing the murine IGHG2A*01 (V00825, IMGT Database) or murine IGLC1 or IGKC constant regions (respectively A0A0G2JE99 and P01837, UniProt).

The recombinant production of ATA mAbs by transfection of the vectors into Freestyle™ 293-F cells (Gibco) as well as the subsequent purification of IgG from culture supernatant using a 1ml HiTrap® Protein G HP affinity column (GE Healthcare) was performed as described previously[4]. A negative control human-derived citrullinated protein-reactive mAb (1F2) was obtained using a similar procedure as described above for the ATA mAbs[4]. Purity and integrity of the generated mAbs was validated by gel electrophoresis.

Gel electrophoresis

The purity and integrity of TOP1, TOP1cc and of the ATA mAbs was assessed by sodium

dodecyl sulfate polyacrylamide gel electrophoresis (SDS-PAGE). TOP1 and TOP1cc were loaded on a polyacrylamide gel with a 4-15% gradient (Bio-Rad) upon addition of Laemmli buffer (Bio-Rad). The ATA mAbs were loaded on a polyacrylamide gel with a 4-15% gradient upon incubation for five minutes at 95°C in Laemmli buffer in presence (reduced) or absence (non-reduced) of 2% β-mercaptoethanol (Merck). PageRuler™ Plus Prestained Protein ladder (ThermoFisher Scientific) was used as reference. Proteins were separated for 60-90 minutes at 100-120 volt. Gels were subsequently washed in Milli-Q water for 5 minutes and stained for one hour using InstantBlue® Coomassie Protein Stain (Abcam). Upon overnight destaining in Milli-Q, gels were visualized using a ChemiDoc™ Touch Imaging system (Bio-Rad).

Western blotting

Western blotting was used to determine the reactivity of ATA mAbs towards TOP1. Gel electrophoresis was performed as described above with 1µg of TOP1. Upon running the gel, gels were blotted on a polyvinylidene difluoride membrane (Bio-Rad). Membrane was blocked with 3% skim milk powder (Sigma) in 0.05% Tween in PBS. Subsequently, 1µg/ml of ATA mAb was added to the membrane and incubated overnight at 4°C. Upon washing the membrane, rabbit anti-human IgG (1:2000, P0214, DAKO) was used as secondary antibody. Washed membranes were developed using Pierce™ enhanced chemiluminescence substrate (ThermoFisher Scientific) and visualized using a ChemiDoc™ Touch Imaging system (Bio-Rad).

Cross-inhibition ELISA with ATA mAbs

Cross-inhibition ELISAs using ATA mAbs with murine and human constant domains were performed to determine whether ATA mAbs can affect the binding of other ATA mAbs to TOP1. To this end, the anti-TOP1-IgG ELISA was adapted by the addition of ATA mAbs with murine constant domains in a serial dilution to the plates before sample addition. Upon washing the plates, ATA mAbs with human constant domains were added and the anti-TOP1-IgG ELISA was conducted as described above.

Mass photometry

Mass photometry was used to determine the stoichiometry of the interaction between the ATA mAbs to TOP1 and TOP1cc. ATA mAbs were incubated at a concentration of 100nM with an excess of TOP1 or TOP1cc for five minutes at room temperature. Subsequently, samples were diluted fivefold in PBS and analyzed using a OneMP mass photometer (Refeyn) as described previously[5,6]. The analysis was conducted on custom-prepared sample carrier slides made from reusable cell culture gaskets (Grace Biolabs) and microscope coverslips (24mm x 50mm, Paul Marienfeld GmbH). Samples were recorded with AcquireMP software (Refeyn) for 60 seconds at a scan rate of 90 fragments per second using the medium field of view. In addition to the protein mixtures, ATA mAbs, TOP1 and TOP1cc were also measured separately at a final concentration of 20nM to determine the molecular mass of the individual components. An in-house standard mix consisting of IgM (1006 kDa), apoferritin (513 kDa), IgG (149 kDa), IgG half-body (73 kDa) was used to perform mass calibration. Calibrated data were then exported and processed using a custom Python pipeline, incorporating seaborn, SciPy, NumPy, pandas and Matplotlib[7–11]. Mass histograms were generated with 5kDa bin widths and resulting mass distributions

were manually annotated. SciPy was further used to analyze the mass histograms, to identify peaks corresponding to the different molecular species, and to estimate the molecular weights of the observed peaks.

TOP1-mediated DNA relaxation assay

A TOP1-mediated DNA relaxation assay was used to study the effect of the ATA mAbs on the enzymatic function of TOP1. To this end, a 10µl suspension containing 1µg/ml TOP1 with a 8x or 32x molar equivalent of ATA mAb in reaction buffer (40mM Tris-HCl, 300mM KCl, 2mM EDTA, 2mM DTT, 100µg/ml BSA) was incubated for one hour at room temperature. Subsequently, 10µl of 20µg/ml negatively supercoiled pUC19 DNA plasmid (ThermoFisher Scientific) was added before performing the enzymatic reaction for 30 minutes at 37°C. Afterwards, 10µl of 2.5% SDS was added and the mixture was incubated at 37°C for 15 minutes. Reaction mixture was mixed with Orange G loading dye (Merck) and ran on a 1% agarose gel at 100 volt for 2-3 hours. GeneRuler 1kb Plus DNA ladder (ThermoFisher Scientific) was used as reference. DNA in the gel was stained using Nancy-520 (Merck). Gel was visualized using a ChemiDoc™ MP Imaging system (Bio-Rad).

References in Supplementary Materials:

1 Slot, L. M. *et al*. Light chain skewing in autoantibodies and B-cell receptors of the citrullinated antigen-binding B-cell response in rheumatoid arthritis. *PLoS One* **16**, e0247847 (2021).

2 Koning, M. T. *et al*. ARTISAN PCR: rapid identification of full-length immunoglobulin rearrangements without primer binding bias. *Br J Haematol* **178**, 983–986 (2017).

3 Giudicelli, V., Brochet, X. & Lefranc, M. P. IMGT/V-QUEST: IMGT standardized analysis of the immunoglobulin (IG) and T cell receptor (TR) nucleotide sequences. *Cold Spring Harb Protoc* **2011**, 695–715 (2011).

4 Kissel, T. *et al*. Antibodies and B cells recognising citrullinated proteins display a broad cross-reactivity towards other post-translational modifications. *Ann Rheum Dis* **79**, 472–480 (2020).

5 Yin, V. *et al*. Probing affinity, avidity, anticooperativity, and competition in antibody and receptor binding to the SARS-CoV-2 spike by single particle mass analyses. *ACS Cent Sci* **7**, 1863–1873 (2021).

6 den Boer, M. A. *et al*. Comparative analysis of antibodies and heavily glycosylated macromolecular immune complexes by size-exclusion chromatography multi-angle light scattering, native charge detection mass spectrometry, and mass photometry. *Anal Chem* **94**, 892–900 (2022).

7 Virtanen, P. *et al*. SciPy 1.0: fundamental algorithms for scientific computing in Python. *Nat Methods* **17**, 261–272 (2020).

8 Waskom, M. L. seaborn: statistical data visualization. *The Journal of Open Source Software* **6**, 3021 (2021).

9 Hunter, J. D. Matplotlib: a 2D graphics environment. *Comput Sci Eng* **9**, 90–95 (2007).

10 McKinney, W. Data Structures for Statistical Computing in Python. *SciPy Proceedings* **445**, 56–61 (2010).

11 Van Der Walt, S., Colbert, S. C. & Varoquaux, G. The NumPy array: a structure for efficient numerical computation. *Comput Sci Eng* **13**, 22–30 (2011).